J|A|C|S
ARTICLES

Published on Web 02/27/2009

Proximity and Cooperativity Effects in Binuclear d^0 Olefin Polymerization Catalysis. Theoretical Analysis of Structure and Reaction Mechanism

Alessandro Motta, Ignazio L. Fragalà,*,† and Tobin J. Marks*,‡

Dipartimento di Scienze Chimiche, Università di Catania, and INSTM, UdR Catania, Viale A. Doria 6, 95125 Catania, Italy, and Department of Chemistry, Northwestern University, Evanston, Illinois 60208-3113

Received September 30, 2008; E-mail: lfragala@dipchi.unict.it; t-marks@northwestern.edu

Abstract: This contribution focuses on the distinctive center-to-center cooperative catalytic properties exhibited by bimetallic "constrained geometry catalysts" (CGCs), and analyzes metal−metal proximity effects on ethylene polymerization processes mediated by (μ-CH_2-3,3′){(η^5-indenyl)[1-H_2Si(^{t}BuN)](ZrMe_2)}$_2$ (**Zr$_2$**)-derived catalysts using density functional theory. Precatalyst geometries are first discussed, and then ion-pair formation/heterolytic dissociation processes involving the binuclear bis(borane) cocatalyst 1,4-(C_6F_5)$_2$BC_6F_4B(C_6F_5)$_2$ (**BN$_2$**), are analyzed and compared with those in the parent mononuclear analogue. It is found that, on proceeding from the mononuclear to binuclear catalyst system, ion-pair dissociation energies increase due to the stronger catalyst center-counterdianion interactions. Moreover, in the binuclear case, the interaction energies are markedly sensitive to geometrical matching between the binuclear bis(borane) and the precatalyst Zr−methyl positions. Binuclear catalytic effects between the metal centers are then explored, with the specific contribution from the proximity of the second metal center. Possible agostic interactions of α-alkenes π-coordinated to one Zr center with the second Zr center of the binuclear catalyst are scrutinized for the case of 1-octene. It is argued that these agostic interactions are at least partly responsible for the unusual enchainment properties of the bimetallic catalysts. In particular, the greater polyethylene product branch densities found experimentally for the bimetallic catalysts can be correlated with an intramolecular reinsertion process, assisted by agostic interactions. Moreover, these same agostic interactions involving a chain growing at one metal site with the second metal site of the binuclear catalyst modify the environment to increase propagation/termination rate ratios, in turn favoring increased product molecular weight (M_n). These effects are observed experimentally at closer Zr···Zr proximities in olefin polymerizations mediated by binuclear CGC catalysts.

Introduction

Enzymatic catalysts are known to achieve superior activity and selectivity, in part as a consequence of their tendency to create high local substrate concentrations and distinctive, conformationally advantaged active site−substrate binding proximities and interactions.[1] These exceptional characteristics have spurred intense recent research efforts focused on discovering unique/more efficient abiotic catalytic processes benefiting from cooperative effects between proximate functional groups[2] or active metal centers in multinuclear catalytic assemblies,[3] to ultimately mimic enzyme catalytic characteristics. Regarding single-site olefin polymerization catalysis,[4,5] research during the past several years has revealed striking cooperativity modalities in binuclear single-site catalysts active for the homo- and

† Università di Catania, and INSTM.
‡ Northwestern University.

(1) (a) Bauer-Siebenlist, B.; Decher, S.; Meyer, F. *Chem.-Eur. J.* **2005**, *11*, 5343–5352. (b) Collman, J. P.; Boulatov, R.; Sunderland, C. J.; Fu, L. *Chem. Rev.* **2004**, *104*, 561–588. (c) Krishnan, R.; Voo, J. K.; Riordan, C. G.; Zahkarov, L.; Rheingold, A. L. *J. Am. Chem. Soc.* **2003**, *125*, 4422–4423. (d) Bruice, T. C. *Acc. Chem. Res.* **2002**, *35*, 139–148. (e) Bruice, T. C.; Benkovic, S. J. *Biochemistry* **2000**, *39*, 6267–6274, and references therein. (f) O'Brien, D. P.; Entress, R. M. N.; Matthew, A. C.; O'Brien, S. W.; Hopkinson, A.; Williams, D. H. *J. Am. Chem. Soc.* **1999**, *121*, 5259–5265. (g) Carazo-Salas, R. E.; Guarguaglini, G.; Gruss, O. J.; Segref, A.; Karsenti, E.; Mattaj, L. W. *Nature* **1999**, *400*, 178–181. (h) Menger, F. M. *Acc. Chem. Res.* **1993**, *26*, 206–212, and references therein. (i) Page, M. I. In *The Chemistry of Enzyme Action*; Page, M. I., Ed.; Elsevier: New York, 1984; pp 1−54.

(2) (a) Zuend, S. J.; Jacobsen, E. N. *J. Am. Chem. Soc.* **2007**, *129*, 15872–15883. (b) Lalonde, M. P.; Chen, Y.; Jacobsen, E. N. *Angew. Chem., Int. Ed.* **2006**, *45*, 6366–6370. (c) Sammis, G. M.; Danjo, H.; Jacobsen, E. N. *J. Am. Chem. Soc.* **2004**, *126*, 9928–9929. (d) Konsler, R. G.; Karl, J.; Jacobsen, E. N. *J. Am. Chem. Soc.* **1998**, *120*, 10780–10781.

(3) (a) Feng, G.; Natale, D.; Prabaharan, R.; Mareque-Rivas, J. C.; Williams, N. H. *Angew. Chem., Int Ed.* **2006**, *45*, 7056–7059. (b) Martin, M.; Sola, E.; Tejero, S.; Lopez, J. A.; Oro, L. A. *Chem.-Eur. J.* **2006**, *12*, 4057–4068. (c) Trost, B. M.; Jaratjaroonphong, J.; Reutrakul, V. *J. Am. Chem. Soc.* **2006**, *128*, 2778–2779. (d) Iranzo, O.; Kovalevsky, A. Y.; Morrow, J. R.; Richard, J. P. *J. Am. Chem. Soc.* **2003**, *125*, 1988–1993. (e) Trost, B. M.; Mino, T. *J. Am. Chem. Soc.* **2003**, *125*, 2410–2411. (f) Jacobsen, E. N. *Acc. Chem. Res.* **2000**, *33*, 421–431. (g) Molenveld, P.; Engbersen, J. F. J.; Reinhoudt, D. N. *Chem. Soc. Rev.* **2000**, *29*, 75–86. (h) Molenveld, P.; Kapsabelis, S.; Engbersen, J. F. J.; Reinhoudt, D. N. *J. Am. Chem. Soc.* **1997**, *119*, 2948–2949. (i) Matthews, R. C.; Howell, D. H.; Peng, W.-J.; Train, S. G.; Treleaven, W. D.; Stanley, G. G. *Angew. Chem., Int. Ed. Engl.* **1996**, *35*, 2253–2256. (j) Sawamura, M.; Sudoh, M.; Ito, Y. *J. Am. Chem. Soc.* **1996**, *118*, 3309–3310.

 10.1021/ja8077208 CCC: $40.75

Chart 1

Scheme 1. Proposed Pathway for Ethyl Branch Formation in Ethylene Homopolymerization Mediated by Binuclear Catalysts

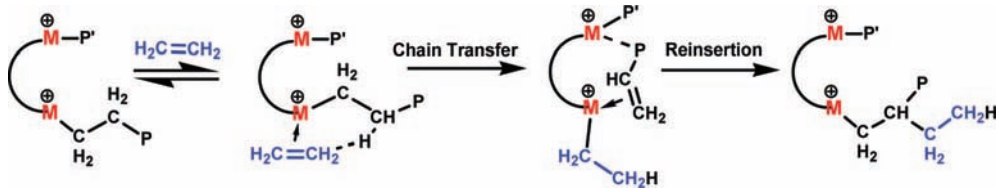

heteropolymerization of ethylene[4a,6] and styrene.[4a,7] In particular, binuclear catalysts having constrained geometry ligation (Chart 1) exhibit significant enhancements (via modification of chain transfer pathway kinetics) of the chain branching in ethylene homopolymerization and significantly enhanced comonomer enchainment selectivity in ethylene−α-olefin copolymerizations versus the mononuclear analogues.[8] These cooperative effects have been shown to be significantly sensitive to the size and the flexibility of the bridging fragment (**X**) and to the nature of the cocatalyst.[6a,b,7,9,10]

An attractive working rationale for these effects invokes cooperative interactions between the propagating chain bound to one metal center and the second center of the binuclear catalyst.[6,8,9] The enhanced selectivity for ethyl branching observed in the bimetallic systems would then arise from a direct β-H chain transfer from the growing polymer chain to coordinated/activated ethylene (chain transfer to monomer), followed by a reinsertion process. Here, the vinylic macromonomer produced at one catalytic center would be stabilized by an agostic interaction with the proximate catalytic center, thus enhancing the probability of subsequent intramolecular re-enchainment with 1,2-regiochemistry at the proximate Zr−ethyl catalytic site (Scheme 1). Moreover, it is well-established that this particular type of β-hydride transfer process represents an important, and in some cases dominant, chain termination pathway in single-site ethylene and propylene homopolymerization.[11−13] The significantly enhanced molecular weight of the polymeric product in $\mathbf{Zr_2}$- vs $\mathbf{Zr_1}$-mediated ethylene homopolymerizations[9]

(4) For reviews of single-site olefin polymerization, see: (a) Amin, S. B.; Marks, T. J. *Angew. Chem., Int. Ed.* **2008**, *47*, 2006–2025. (b) Vanka, K.; Xu, Z.; Seth, M.; Ziegler, T. *Top. Catal.* **2005**, *34*, 143–164. (c) Kaminsky, W. *J. Polym. Sci., Part A: Polym. Chem.* **2004**, *42*, 3911–3921. (d) Bochmann, M. *J. Organomet. Chem.* **2004**, *689*, 3982–3998. (e) Gibson, V. C.; Spitzmesser, S. K. *Chem. Rev.* **2003**, *103*, 283–316. (f) Pedeutour, J.-N.; Radhakrishnan, K.; Cramail, H.; Deffieux, A. *Macromol. Rapid Commun.* **2001**, *22*, 1095–1123. (g) Gladysz, J. A. *Chem. Rev.* **2000**, *100* (special issue on "Frontiers in Metal-Catalyzed Polymerization"). (h) Marks, T. J.; Stevens, C. J. *Top. Catal.* **1999**, *7* (special volume on Advances in Polymerization Catalysis, Catalysts and Processes). (i) Britovsek, G. J. P.; Gibson, V. C.; Wass, D. F. *Angew. Chem., Int. Ed.* **1999**, *38*, 428–447. (j) Kaminsky, W.; Arndt, M. *Adv. Polym. Sci.* **1997**, *127*, 144–187. (k) Bochmann, M. *J. Chem. Soc., Dalton Trans.* **1996**, 255–270. (l) Brintzinger, H.-H.; Fischer, D.; Mülhaupt, R.; Rieger, B.; Waymouth, R. M. *Angew. Chem., Int. Ed.* **1995**, *34*, 1143–1170. (m) *Catalyst Design for Tailor-Made Polyolefins*; Soga, K., Terano, M., Eds.; Elsevier: Tokyo, 1994. (n) Marks, T. J. *Acc. Chem. Res.* **1992**, *25*, 57–65.

(5) (a) Marks, T. J. *Proc. Nat. Acad. Sci. U.S.A.* **2006**, *103* (Special Feature on Polymerization). (b) Severn, J. R.; Chadwick, J. C.; Duchateau, R.; Friederichs, N. *Chem. Rev.* **2005**, *105*, 4073–4147. (c) Arndt, S.; Okuda, J. *Chem. Rev.* **2002**, *102*, 1953–1976. (d) Chum, P. S.; Kruper, W. J.; Guest, M. J. *Adv. Mater.* **2000**, *12*, 1759–1767. (e) McKnight, A. L.; Waymouth, R. M. *Chem. Rev.* **1998**, *98*, 2587–2598. (f) Harrison, D.; Coulter, I. M.; Wang, S. T.; Nistala, S.; Kuntz, B. A.; Pigeon, M.; Tian, J.; Collins, S. *J. Mol. Catal. A: Chem.* **1998**, *128*, 65–77. (g) Soga, K.; Shiono, T. *Prog. Polym. Sci.* **1997**, *22*, 1503–1546. (h) Soga, K.; Uozumi, T.; Nakamura, S.; Toneri, T.; Teranishi, T.; Sano, T.; Arai, T.; Shiono, T. *Macromol. Chem. Phys.* **1996**, *197*, 4237–4251. (i) Devore, D. D.; Timmers, F. J.; Hasha, D. L.; Rosen, R. K.; Marks, T. J.; Deck, P. A.; Stern, C. L. *Organometallics* **1995**, *14*, 3132–3134.

(6) For studies of binuclear polymerization catalysis, see: (a) Guo, N.; Stern, C. L.; Marks, T. J. *J. Am. Chem. Soc.* **2008**, *130*, 2246–2261. (b) Review: Li, H.; Marks, T. J. *Proc. Natl. Acad. Sci. U.S.A.* **2006**, *103*, 15295–15302. (c) Li, H.; Li, L.; Marks, T. J. *Angew. Chem., Int. Ed.* **2004**, *37*, 4937–4940. (d) Green, M. L. H.; Popham, N. H. *J. Chem. Soc., Dalton Trans.* **1999**, 1049–1059, and references therein. (e) Spaleck, W.; Kuber, F.; Bachmann, B.; Fritze, C.; Winter, A. *J. Mol. Catal. A: Chem.* **1998**, *128*, 279–287. (f) Yan, X.; Chernega, A.; Green, M. L. H.; Sanders, J.; Souter, J.; Ushioda, T. *J. Mol. Catal. A: Chem.* **1998**, *128*, 119–141. (g) Soga, K.; Ban, H. T.; Uozumi, T. *J. Mol. Catal. A: Chem.* **1998**, *128*, 273–278. (h) Bochmann, M.; Cuenca, T.; Hardy, D. T. *J. Organomet. Chem.* **1994**, *484*, C10–C12.

(7) Noh, S. K.; Jung, W.; Oh, H.; Lee, Y. R.; Lyoo, W. S. *J. Organomet. Chem.* **2006**, 5000–5006.

(8) (a) Wang, J.; Li, H.; Guo, N.; Li, L.; Stern, C. L.; Marks, T. J. *Organometallics* **2004**, *23*, 5112–5114. (b) Guo, N.; Li, L.; Marks, T. J. *J. Am. Chem. Soc.* **2004**, *126*, 6542–43. (c) Li, H.; Li, L.; Marks, T. J.; Liable-Sands, L.; Rheingold, A. L. *J. Am. Chem. Soc.* **2003**, *124*, 10788–10789. (d) Noh, S. K.; Lee, J.; Lee, D. *J. Organomet. Chem.* **2003**, *667*, 53–60. (e) Li, L.; Metz, M. V.; Li, H.; Chen, M.-C.; Marks, T. J.; Liable-Sands, L.; Rheingold, A. L. *J. Am. Chem. Soc.* **2002**, *124*, 12725–12741. (f) Abramo, G. P.; Li, L.; Marks, T. J. *J. Am. Chem. Soc.* **2002**, *124*, 13966–13967.

(9) (a) Li, H.; Li, L.; Schwartz, D. J.; Metz, M. V.; Marks, T. J.; Liable-Sands, L.; Rheingold, A. L. *J. Am. Chem. Soc.* **2005**, *127*, 14756–14768. (b) Li, H.; Stern, C. L.; Marks, T. J. *Macromolecules* **2005**, *38*, 9015–9027.

(10) (a) Yuen, H. F.; Marks, T. J. *Organometallics* **2008**, *27*, 155–158. (b) Salata, M. R.; Marks, T. J. *J. Am. Chem. Soc.* **2008**, *130*, 12–13.

(11) For discussions of chain transfer mechanisms in single-site propylene polymerization, see: (a) Liu, Z.; Somsook, E.; White, C. B.; Rosaaen, K. A.; Landis, C. R. *J. Am. Chem. Soc.* **2001**, *123*, 11193–11207. (b) Lin, S.; Tagge, C. D.; Waymouth, R. M.; Nele, M.; Collins, S.; Pinto, J. C. *J. Am. Chem. Soc.* **2000**, *122*, 11275–11285. (c) Veghini, D.; Henling, L. M.; Burkhardt, T. J.; Bercaw, J. E. *J. Am. Chem. Soc.* **1999**, *121*, 564–573. (d) Stehling, U.; Diebold, J.; Kirsten, R.; Röll, W.; Brintzinger, H. H.; Jungling, S.; Mülhaupt, R.; Langhauser, F. *Organometallics* **1994**, *13*, 964–970.

also suggests that termination rates may be depressed. Such effects find an attractive rationale in cooperative reactivity patterns involving two metal centers that would coordinate/stabilize the growing polymer chain, possibly via β-agostic interactions (e.g., Structure **I** and the intermediates depicted in Scheme 1). Such proximity effects could reasonably impede chain transfer to monomer and subsequent macromonomer dissociation as a chain termination pathway, thereby reducing the overall chain termination rate and enhancing the rate of branch-forming macromonomer re-enchainment (Scheme 1).

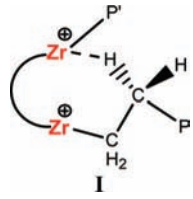

I

In this context, further detailed understanding of the unique properties of binuclear olefin polymerization catalysts would benefit directly from theoretical modeling, which offers an incisive tool for analyzing binuclear catalytic reaction coordinates. For processes mediated by group 4 metallocenium catalysts, quantum chemical modeling has played a fundamental role in elucidating propagation and chain transfer mechanisms, the effects of metal identity and ligand substituents,[14] and finally, the role of counteranions and solvation on enchainment kinetics and catalyst thermodynamics[15,16] as well as on regio- and stereocontrol in propene[16] and styrene insertion.[17]

The present study represents the first theoretical analysis of the salient mechanistic features associated with proximity effects on enchainment processes in binuclear olefin polymerization catalysis. Details of the precatalyst geometries and the relevant ion-pair formation/heterolytic dissociation processes are first analyzed. Next, the nature of the interactions of a vinyl-terminated oligoethylene model fragment involving both sites of the binuclear catalyst and the effects of such interactions on polymerization pathways are scrutinized. Comparisons to the mononuclear analogue highlight the origins of the distinctive reactivity features associated with these binuclear catalytic systems. Here (μ-CH_2-3,3′){(η^5-indenyl)[1-H_2Si(^{t}BuN)]-($ZrMe_2$)}$_2$ (**Zr_2**) has been adopted as the bimetallic model precatalyst for ethylene polymerization processes, with mononuclear **Zr_1** serving as the control. Propagation and termination process are compared and contrasted in the binuclear and mononuclear cases, to better understand the observed metal−metal cooperativity effects on product polyethylene microstructure and molecular weight. It will be seen that the two proximate Zr electrophilic centers can engage in distinctive binuclear interactions with olefinic substrates and that these can significantly influence catalytic enchainment and chain transfer processes.

Computational Details

Calculations were performed at the level of the B3LYP formalism. The effective core potential (ECP) of Hay and Wadt,[18] which explicitly treats 4s and 4p electrons and a basis set contracted as [4s,4p,4d], were used for the zirconium atom. The standard all-electron 6-31G** basis was used for the remaining atoms.[19] Molecular geometry optimization of stationary points used analytical gradient techniques. The transition state was searched with the synchronous, transit-guided quasi-Newton method.[20] In two cases (the Zr_2-^{n}octyl system for both insertion and chain transfer), however, this method did not converge, and the "distinguished reaction coordinate procedure" was used in the analysis of the transition-state geometry along the emerging C−C σ-bond for the insertion pathway, and along the emerging H−C σ-bond for the chain transfer pathway. The enthalpies (ΔH) reported are potential energy differences without zero point or vibrational finite temperature corrections. These terms are far too expensive to calculate for the size of the systems considered here. Moreover, it has been reported[15b] that these corrections are expected to be on the order of 2−3 kcal/mol and, hence, represent only a slight refinement of the electronic potential energy values. Finally, it is expected that very similar corrections will apply for all the systems compared, thus affecting the calculated relative trends in a very minor way. All calculations were performed using G03[21] codes on IBM-SP systems.

Results and Discussion

In this section, we discuss proximity effects in the various polymerization catalytic site configurations by first comparing the **Zr_1** and **Zr_2** precatalysts with the structures of the corresponding naked cations. The ion-pair formation and heterolytic

(12) For discussions of chain transfer mechanisms in single-site ethylene polymerization, see: (a) Izzo, L.; Riccardis, F. D.; Alfano, C.; Caporaso, L.; Oliva, L. *Macromolecules* **2001**, *34*, 2–4. (b) Wang, L.; Yuan, Y.; Feng, L.; Wang, Y.; Pan, J.; Ge, C.; Ji, B. *Eur. Polym. J.* **2000**, *36*, 851–855. (c) Izzo, L.; Caporaso, L.; Senatore, G.; Oliva, L. *Macromolecules* **1999**, *32*, 6913–6916.

(13) For theoretical studies of single-site chain transfer pathways, see: (a) Yang, S.-Y.; Ziegler, T. *Organometallics* **2006**, *25*, 887–900. (b) Thorshaug, K.; Stovneng, J. A.; Rytter, E.; Ystenes, M. *Macromolecules* **1998**, *31*, 7149–7165. (c) Klesing, A.; Bettonville, S. *Phys. Chem. Chem. Phys.* **1999**, *1*, 2373–2377. (d) Froese, R. D. J.; Musaev, D. G.; Morokuma, K. *Organometallics* **1999**, *18*, 373–379. (e) Margl, P. M.; Woo, T. K.; Ziegler, T. *Organometallics* **1998**, *17*, 4997–5002.

(14) (a) Zhu, C.; Ziegler, T. *Inorg. Chim. Acta* **2003**, *345*, 1–7. (b) Froese, R. D. J.; Musaev, D. G.; Morokuma, K. *Organometallics* **1999**, *18*, 373–379. (c) Musaev, D. G.; Froese, R. D. J.; Morokuma, K. *New J. Chem.* **1997**, *21*, 1269–1282. (d) Koga, N.; Yoshida, T.; Morokuma, K. *Ziegler Catalysts: recent scientific innovations and technological improvements*; Fink, G., Muelhaupt, R., Brintzinger, H. H., Eds.; Springer: Berlin, Germany, 1995; pp 275−289. (e) Fan, L.; Harrison, D.; Woo, T. K.; Ziegler, T. *Organometallics* **1995**, *14*, 2018–2026.

(15) (a) Zurek, E.; Ziegler, T. *Prog. Polym. Sci.* **2004**, *29*, 107–148. (b) Xu, Z.; Vanka, K.; Firman, T.; Michalak, A.; Zurek, E.; Zhu, C.; Ziegler, T. *Organometallics* **2002**, *21*, 2444–2453. (c) Ystenes, M.; Eilertsen, J. L.; Liu, J.; Ott, M.; Rytter, E.; Stovneng, J. A. *J. Polym. Sci. Pol. Chem.* **2000**, *38*, 3450. (d) Xu, Z.; Vanca, K.; Ziegler, T. *Macromol. Symp.* **2004**, *206*, 457–469. (e) Wondimagegn, T.; Xu, Z.; Vanca, K.; Ziegler, T. *Organometallics* **2004**, *23*, 3847–3852.

(16) (a) Motta, A.; Fragalà, I. L.; Marks, T. J. *J. Am. Chem. Soc.* **2007**, *129*, 7327–7338. (b) Caporaso, L.; Gracia-Budria, J.; Cavallo, L. *J. Am. Chem. Soc.* **2006**, *128*, 16649–16654. (c) Guerra, G.; Corradini, P.; Cavallo, L. *Macromolecules* **2005**, *38*, 3973–3976. (d) Milano, G.; Fiorello, G.; Guerra, G.; Cavallo, L. *Macromol. Chem. Phys.* **2002**, *203*, 1564–1572. (e) Petitjean, L.; Pattou, D.; Ruiz-Lopez, M.-F. *THEOCHEM* **2001**, *541*, 227–235. (f) Moscardi, G.; Resconi, L.; Cavallo, L. *Organometallics* **2001**, *20*, 1918–1931. (g) Resconi, L.; Cavallo, L.; Fait, L.; Fait, A.; Piemontesi, F. *Chem. Rev.* **2000**, *100*, 1253–1345. (h) Lanza, G.; Fragalà, I. L.; Marks, T. J. *J. Am. Chem. Soc.* **2000**, *122*, 12764–12777. (i) Moscardi, G.; Piemontesi, F.; Resconi, L. *Organometallics* **1999**, *18*, 5264–5275. (j) Lanza, G.; Fragalà, I. L.; Marks, T. J. *J. Am. Chem. Soc.* **1998**, *120*, 8257–8259. (k) Morokuma, K.; Yoshida, T.; Koga, N.; Musaev, D. G. *Polym. Mater. Sci. Eng.* **1996**, *74*, 425–435. (l) Castonguay, L. A.; Rappé, A. K. *J. Am. Chem. Soc.* **1992**, *114*, 5832–5842.

(17) (a) Yang, S. H.; Huh, J.; Jo, W. H. *Organometallics* **2006**, *25*, 1144–1150. (b) Yang, S. H.; Huh, J.; Yang, J. S.; Jo, W. H. *Macromolecules* **2004**, *37*, 5741–5751.

(18) Hay, P. J.; Wadt, W. R. *J. Chem. Phys.* **1985**, *82*, 299–310.

(19) (a) Hehre, W. J.; Ditchfield, R.; Pople, J. A. *J. Chem. Phys.* **1972**, *56*, 2257–2261. (b) Francl, M. M.; Pietro, W. J.; Hehre, W. J.; Binkley, J. S.; Gordon, M. S.; DeFrees, D. J.; Pople, J. A. *J. Chem. Phys.* **1982**, *77*, 3654–3665.

(20) Peng, C.; Schlegel, H. B. *Isr. J. Chem.* **1993**, *33*, 449–454.

(21) Frisch, M. J.; et al. *Gaussian 03, Revision A.1*; Gaussian, Inc.: Pittsburgh, PA, 2003.

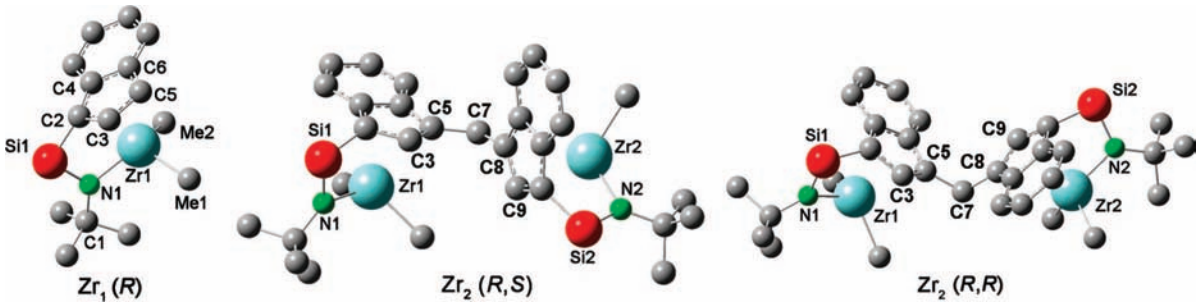

Figure 1. Structures of the $\mathbf{Zr_1}$ mononuclear and $\mathbf{Zr_2}$ binuclear precatalysts.

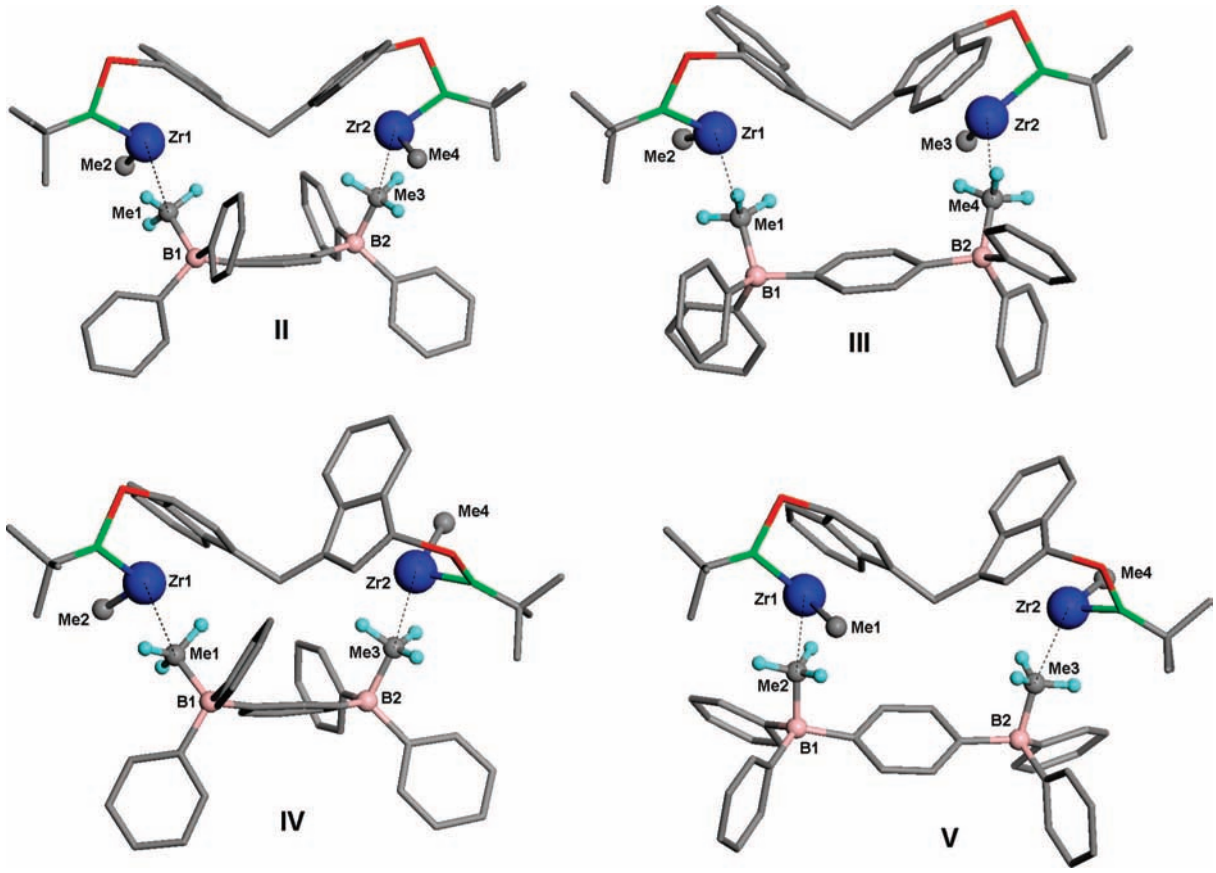

Figure 2. Possible structures formed via bifunctional organoborane $\mathbf{BN_2}$ Zr−CH_3 abstraction from the binuclear CGC catalyst *R,R* diastereoisomer (Structures **II** and **III**) and from the *R,S* diastereoisomer (Structures **IV** and **V**) of the $\mathbf{Zr_2}$ system.

dissociation processes with the binuclear bis(borane) cocatalyst 1,4-$(C_6F_5)_2BC_6F_4B(C_6F_5)_2$ ($\mathbf{BN_2}$) are then analyzed in the case of the $\mathbf{Zr_2}$ systems, and the results are compared/contrasted with those for the mononuclear analogue. As the next step, the agostic interactions between the vinyl-terminated organic fragment and the two metallic centers of the binuclear catalyst are scrutinized. Finally, the effects of the internuclear proximity on the kinetics of the polymerization propagation and termination steps are analyzed and the results are compared with experiment.

Precatalyst and Naked Cation Molecular Structures. Figure 1 shows the optimized structures of the $\mathbf{Zr_1}$ and $\mathbf{Zr_2}$ precatalysts. For the $\mathbf{Zr_2}$ systems, two diastereoisomeric configurations are possible, namely *R,R* and *R,S*, due to the mutual orientations of the indenyl rings. The *R,R* diastereoisomer exhibits C_2 symmetry, while the *R,S* diastereoisomer is C_1 symmetric. The two diastereoisomers are found to be comparable in energy. In principle, the $\mathbf{Zr_2}$ molecule can undergo rotation about the −X− linking bridge and, therefore, multiple starting geometries were screened to investigate the different possible conformations of this precatalyst. A unique conformational energetic minimum is located for each diastereoisomer in which the two indenyl rings are forced into a twisted conformation by steric repulsions arising from the close proximity of the two metal−ligand centers, connected by the -CH_2- bridge (Figure 1). In particular, the *R,S* conformer exhibits two computed minimum energy dihedral angles, C3−C5−C7−C8 and C9−C8−C7−C5, of −9.4° and 93.3°, respectively, while the *R,R* conformer exhibits a single minimized dihedral angle value, C3−C5−C7−C8 = C9−C8−C7−C5, of 86.9° due to the molecular C_2 symmetry (Figure 1). Proximity effects on the coordination environment around the metal centers in both -CH_2- bridged binuclear precatalysts were then compared with the coordination environment in the mononuclear precatalyst. It is found that the proximity of the second CGC-Zr center does not induce significant modifications of the immediate catalyst center geometry. A detailed geometric comparison between the bi-

Scheme 2. Methyl Arrangements in the Diastereoisomeric *R,R* and *R,S* Zr_2 Catalysts

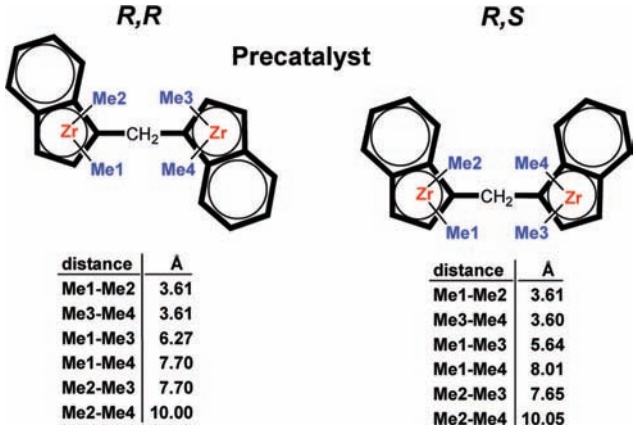

distance	Å
Me1-Me2	3.61
Me3-Me4	3.61
Me1-Me3	6.27
Me1-Me4	7.70
Me2-Me3	7.70
Me2-Me4	10.00

distance	Å
Me1-Me2	3.61
Me3-Me4	3.60
Me1-Me3	5.64
Me1-Me4	8.01
Me2-Me3	7.65
Me2-Me4	10.05

nuclear and mononuclear precatalysts is presented in the SI. The closely comparable metrical parameters for the monomer and binuclear catalysts agree well, in turn, with X-ray diffraction-derived experimental data for the closely analogous single-site complexes characterized previously.[6b,8e,9]

Ion-Pair Interactions. Since it is well established that precatalyst/cocatalyst interactions to form ion pairs play a major role in single-site catalytic activity and selectivity,[4,5,22] a detailed analysis of the possible interaction modes between binuclear precatalyst and binuclear cocatalyst models is performed here. In the present study, the precatalyst is activated via methide abstraction by strongly Lewis-acidic perfluorotriarylborane cocatalysts.[4,5,22] For the mononuclear $\mathbf{Zr_1}$ + **BN** system, the energetic demands of ion-pair creation are partially compensated for by concurrent Zr···F−C(aryl) interactions, evidenced by elongation of one F−C(aryl) bond (1.40 Å) vs the mean F−C(aryl) distance of 1.34 Å for the remaining (aryl)C−F bonds. In the case of the binuclear -CH_2- bridged $\mathbf{Zr_2}$ + $\mathbf{BN_2}$ system, it is possible to abstract two Zr−methyl groups via several pathways. A basic geometrical requirement for abstraction of two Zr−methyls in the binuclear -CH_2- bridged $\mathbf{Zr_2}$ system to yield optimally stable ion pairs is to have comparable distances between the two methyl groups to be abstracted and the distance between the two electron-deficient boron centers (B---B = 6.04 Å) of the bifunctional $\mathbf{BN_2}$ cocatalyst. In this perspective, only two ion-pair product structures for each diastereoisomer are compatible with these constraints. For diastereoisomer *R,R*, one structure (Structure **II** in Figure 2) is obtained via abstraction of Me1 and Me3, while the other (Structure **III** in Figure 2) is obtained via abstraction of Me2 and Me3 (Scheme 2). Similar results are obtained for diastereoisomer *R,S* (structures **IV** and **V** in Figure 2).

(22) (a) Roberts, J. A. S.; Chen, M.-C.; Seyam, A. M.; Li, L.; Zuccaccia, C.; Stahl, N. G.; Marks, T. J. *J. Am. Chem. Soc.* **2007**, *129*, 12713–12733. (b) Chen, M.-C.; Roberts, J. A. S.; Seyam, A. M.; Li, L.; Zuccaccia, C.; Stahl, N. G.; Marks, T. J. *Organometallics* **2006**, *25*, 2833–2850. (c) Stahl, N. G.; Salata, M. R.; Marks, T. J. *J. Am. Chem. Soc.* **2005**, *127*, 10898. (d) Chen, M. C.; Roberts, J. A.; Marks, T. J. *Organometallics* **2004**, *23*, 932–935. (e) Chen, M.-C.; Roberts, J. A.; Marks, T. J. *J. Am. Chem. Soc.* **2004**, *126*, 4605–4625. (f) Zuccaccia, C.; Stahl, N. G.; Macchioni, A.; Chen, M.-C.; Roberts, J. A.; Marks, T. J. *J. Am. Chem. Soc.* **2004**, *126*, 1448–1464. (g) Chen, E. Y.-X.; Marks, T. J. *Chem. Rev.* **2000**, *100*, 1391–1434. (h) Beswick, C. L.; Marks, T. J. *J. Am. Chem. Soc.* **2000**, *122*, 10358–10370. (i) Deck, P. A.; Beswick, C. L.; Marks, T. J. *J. Am. Chem. Soc.* **1998**, *120*, 1772–1784. (j) Jia, L.; Yang, X.-M.; Ishihara, A.; Marks, T. J. *Organometallics* **1995**, *14*, 3135–3137. (k) Jia, L.; Yang, X.-M.; Stern, C. L.; Marks, T. J. *Organometallics* **1994**, *13*, 3755–3757.

Table 1. Ion-Pair Reactant Geometrical Matching Parameter ($\Delta_{matching}$ = |Zr−Zr| − |B−B|, Å), Formation Enthalpies (ΔH_{form}, kcal/mol), and Heterolytic Ion-Pair Separation Enthalpies (ΔH_{ips}, kcal/mol) for Mononuclear $\mathbf{Zr_1}$ and Binuclear $\mathbf{Zr_2}$ Catalysts Paired with Boranes BN and BN_2, Respectively

	structure	$\Delta_{matching}$	ΔH_{form}	ΔH_{ips}
mononuclear		−	−8.9	93.2
R,R	**II**	0.23	−11.8	271.9
	III	1.66	−5.0	261.0
R,S	**IV**	−0.40	−9.5	270.4
	V	1.60	−5.0	261.5

Alternative methyl abstraction pathways are not geometrically feasible, nor are the products as thermodynamically stable, since methyl groups coordinated to the same metal center lie in too close proximity (in all cases the distance is 3.61 Å, Scheme 2) versus the boron−boron distances in bifunctional $\mathbf{BN_2}$ (B---B = 6.04 Å), while the Me2-Me4 distance (10 Å) is too great in each diastereoisomer for favorable abstraction (Scheme 2). Note that in diastereoisomer *R,R*, the Me1-Me4 and the Me2-Me3 positions are identical due to the C_2 symmetry.

Finally, the distance between groups Me1 and Me4 (8.01 Å) in diastereoisomer *R,S* is too long for optimum matching to the bis(borane) centers.

Useful information describing the stability of the ion-pair adducts is derived from analyzing the energetics of the respective formation (eq 1) and heterolytic dissociation processes (eq 2).

$$\text{precatalyst} + \text{cocatalyst} \rightarrow \text{ion pair} + \Delta H_{\text{form}} \quad (1)$$

$$\text{ion pair} \rightarrow \text{naked cation} + \text{counteranion} + \Delta H_{\text{ips}} \quad (2)$$

Table 1 summarizes ion-pair formation (ΔH_{form}) and ion-pair separation (ΔH_{ips}) enthalpies computed for the mono ($\mathbf{Zr_1}$) and the binuclear ($\mathbf{Zr_2}$) complexes with the respective borane cocatalysts, **BN** and $\mathbf{BN_2}$. Note that in the binuclear systems, the ion-pair stabilization energies (assessed in terms of both ΔH_{form} and ΔH_{ips}) depend on optimal geometrical matching of the distance between the abstracted methyl groups of the binuclear precatalyst and that between the boron atoms (6.04 Å) in the bifunctional cocatalyst ($\mathbf{BN_2}$). The closer the geometrical match (similar values), the greater the stabilization of the ion-pair structures. Table 1 shows that the structures with more comparable distances (smaller $\Delta_{matching}$) have both greater ΔH_{form} stabilization values and greater ΔH_{ips} demands.

Naïve considerations would suggest that, all other things being equal, the methyl abstraction process in the binuclear systems should proceed with a ΔH_{form} which is twice that of the mononuclear case since the process involves the abstraction of two Zr−CH_3 groups. However, the computed ΔH_{form} values for the present binuclear structures are found to be comparable to, or even less in magnitude, than those of the corresponding mononuclear complex (Table 1). In the binuclear systems, the two abstraction processes are not independent (hence not additive) since the two active centers of both the binuclear precatalyst ($\mathbf{Zr_2}$) and the bifunctional cocatalyst ($\mathbf{BN_2}$) are constrained by a bridging fragment (a methylene group in $\mathbf{Zr_2}$ and the 1,4-phenylene fragment in $\mathbf{BN_2}$). Moreover, the Lewis acidity of the diborane cocatalyst ($\mathbf{BN_2}$) is likely diminished after abstraction of the first CH_3 group. In fact, the presence of a vicinal negative charge due to the first methyl abstraction inhibits formation of a second negative charge arising from the second abstraction process. Similar considerations apply for the formation of the positive charges localized on the binuclear

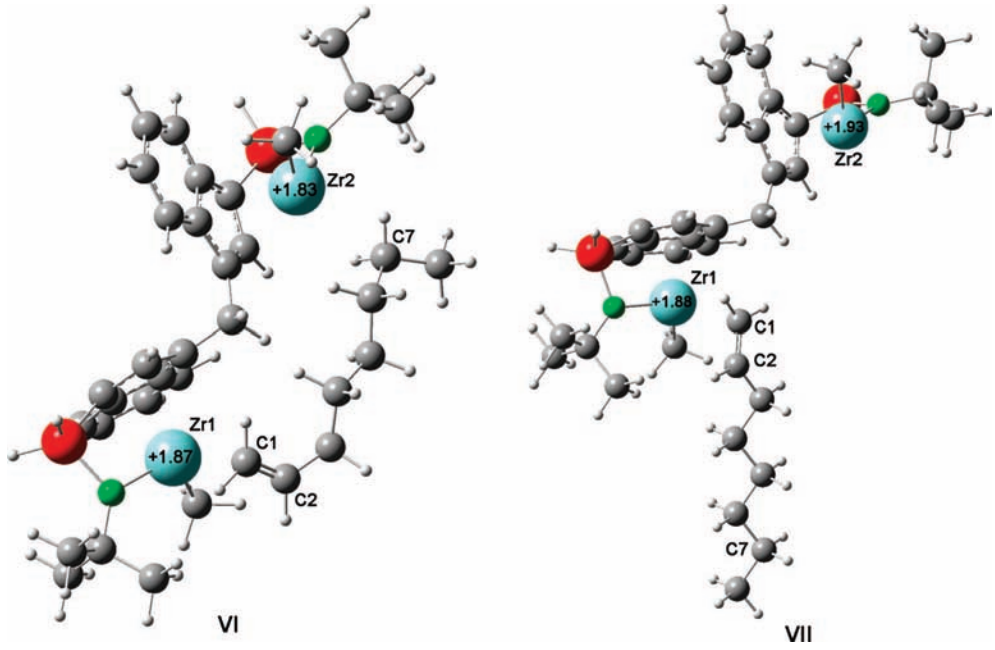

Figure 3. Two different π-complexes of 1-octene with the *R,R* diastereoisomer of the -CH_2- bridged $\mathbf{Zr_2}$ bimetallic dicationic CGC catalyst.

Scheme 3. Pathways for Propagation and Termination in Olefin Polymerization Processes

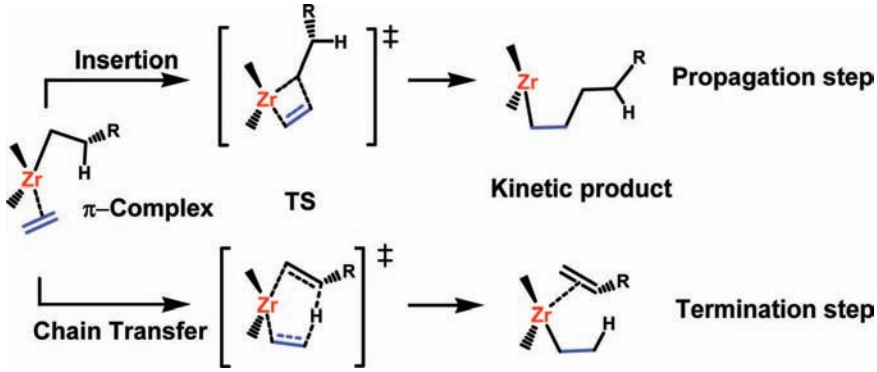

catalyst metal centers. These geometrical and electrostatic constraints that introduce an intrinsic structural destabilization as well as the diminished borane Lewis acidity can be correlated with the computed, modest ΔH_{form} values. In contrast, large differences in ΔH_{ips} values are found on passing from the mononuclear to binuclear systems and reflect the largely electrostatic nature of the $M^+\cdots H_3CB-R^-$ ion-pair interaction,[16h,j,23] and hence, the Coulombic contribution $(2+) \times (2-)$ in binuclear ion pairs that is significantly greater than in the mononuclear $(1+) \times (1-)$ systems. Any deviations from purely electrostatic interactions are reasonably attributable to minor covalent contributions and geometrical distortions. In terms of reactivity, the stronger ion-pair interactions in the binuclear systems as well as their rigidity offer the most plausible origins of generally reduced polymerization activity relative to the mononuclear analogues. It has been demonstrated[23] that the propagation kinetics in homogeneous single-site catalytic polymerization processes are extremely sensitive to the strengths of the ion-pair interactions, since olefin activation/insertion requires displacement of the counteranion.[4,5,23] Larger ion-pair interaction energies (as expressed by ΔH_{ips}) increase the energetic cost in counteranion displacement and, hence, shift the entire olefin insertion enthalpic profile to higher values.

Ethyl Branch Formation. The distinctive selectivity of the binuclear catalytic systems for introducing ethyl branching[9] can be rationalized in terms of a conventional monometallic macromonomer elimination, via a chain transfer process, followed by 1,2-intermolecular reinsertion at the ethyl cation produced by chain transfer (Scheme 1). The oligomeric or polymeric vinyl macromonomer chain produced at one catalytic center by the chain transfer process is thought to be bound/detained by binuclear interactions (presumably agostic) involving the adjacent cationic metal center. The weakly bonded oligomeric/polymeric chain would then have an enhanced probability of intramolecular re-enchainment with 1,2-regiochemistry at the proximate Zr−ethyl$^+$ or Zr−P$^+$ catalytic site (Scheme 1). To understand whether such an interaction of a vinyl-terminated fragment with the binuclear system is energetically favorable during the polymerization process, the interaction between the -CH_2- bridged bimetallic catalyst ($\mathbf{Zr_2}$) and a vinyl-terminated fragment of sufficient dimensions to accommodate the distance between the two $\mathbf{Zr_2}$ sites was modeled. For this purpose, the 1-octene monomer was selected.

Figure 3 shows the two possible structures of a 1-octene π-complex involving the Zr1 center (for the *R,R* diastereoisomer). Note that structure **VI** allows closer proximity of the

Table 2. Computed Geometrical Parameters for the π-Complexes, Insertion Transition States, and Products Arising from the Insertion of Ethylene at $\mathbf{Zr_1}$ Mononuclear and $\mathbf{Zr_2}$ Binuclear Catalyst Systems[a]

	Insertion Pathway		
	$\mathbf{Zr_1}$-^{n}propyl	$\mathbf{Zr_2}$-^{n}propyl	$\mathbf{Zr_2}$-^{n}octyl
		π-Complex	
Zr1−C1	2.836	2.839	2.845
Zr1−C2	2.863	2.857	2.897
Zr1−C3	2.236	2.236	2.245
Zr1−H2	2.318	2.324	2.303
C4−H2	1.141	1.140	1.145
C1−C2	1.348	1.348	1.348
C2−C3	4.145	4.134	4.231
Zr1−C3−C4	91.5	91.6	91.1
		Transition State	
Zr1−C1	2.382	2.379	2.371
Zr1−C2	2.646	2.646	2.642
Zr1−C3	2.290	2.297	2.319
C1−C2	1.401	1.402	1.405
C3−H1	1.134	1.134	1.133
C2−C3	2.289	2.282	2.260
Zr1−C3−H1	68.9	68.6	68.5
		Kinetic Product	
Zr1−C1	2.214	2.213	2.227
Zr1−C2	2.844	2.829	2.969
Zr1−C3	2.769	2.715	3.015
C1−C2	1.555	1.557	1.547
C2−C3	1.557	1.560	1.550
C3−H1	1.121	1.119	1.124
Zr1−C1−C2	96.4	95.7	102.3

[a] Atom labeling refers to Figure 4.

1-octene "tail" to the non-π-bonded metal site (Zr2) and, in particular, the C7−H bond vector is directed toward the Zr2 center and with slight C−H elongation (~0.02 Å) relative to structure **VII** where the same bond remains unperturbed. The NBO population analysis reveals that in structure **VI**, with closer 1-octene contact, the charge localized on Zr1 (+1.87) compares well with that on Zr2 (+1.83). In contrast, for structure **VII,** olefin coordination decreases the positive charge on Zr1 (+1.88) comparably to that in **VI**, however Zr2 remains considerably more electron-deficient (+1.93) than in **VI**. Agostic C−H electron donation to Zr2 in **VI** is clearly responsible for this effect. Moreover, structure **VI** is computed to be 2.0 kcal/mol more stable than structure **VII**. These geometrical and energetic considerations strongly suggest that the proximity of two metal sites in the bimetallic catalysts promotes a non-negligible agostic interaction between an oligomeric π-bonded vinyl-terminated oligoethylene chain and the second metal site, a prerequisite for the proposed ethyl branching mechanism (Scheme 1). Important geometrical issues concerning this interaction are the dimensions of the oligomeric chain that best favor the agostic interaction with the Zr2 metal site.

Indeed, it becomes evident that the intermetallic distance in the $\mathbf{Zr_2}$ catalyst (for the particular *R,R* diastereoisomer investigated) along with the operative nonbonded repulsions requires a linear α-alkene chain having at least seven carbon atoms to form optimally stable agostic interactions. This observation is in accord with the subsequent formation of structures similar to structure **I** (above) that would be expected to enhance product polymer molecular weight as observed experimentally in $\mathbf{Zr_2}$-mediated ethylene homopolymerizations (vide infra). It will be shown below that the aforementioned agostic interactions play an important role in favoring higher molecular weight polymeric product.

Ethylene Polymerization Process. There is experimental evidence that 70× and 130× increases in molecular weight are achieved with $\mathbf{Zr_2}$ versus $\mathbf{C2-Zr_2}$ and $\mathbf{Zr_1}$, respectively, under identical polymerization conditions using $\mathbf{BN_2}$ as the cocatalyst.[9] Note that the use of methylalumoxane as the cocatalyst increases the polyethylene molecular weight produced by binuclear $\mathbf{C2-Zr_2}$ and $\mathbf{Zr_2}$ vs mononuclear $\mathbf{Zr_1}$ by ~600×.[9] In this section, the propagation (Cossee insertion mechanism[24]) and termination (β-hydrogen chain transfer mechanism[12,13]) pathways (Scheme 3) are analyzed and compared in detail to understand how metal proximity can enhance the polyethylene molecular weight achieved with the bimetallic catalysts. In particular, mononuclear ($\mathbf{Zr_1}$) and binuclear -CH_2- bridged ($\mathbf{Zr_2}$) naked cations, having an ^{n}propyl group to model the growing polyethylene chain, are investigated to understand the role of Zr···Zr proximity in the propagation and chain transfer processes. A further calculation on the $\mathbf{Zr_2}$ system uses the ^{n}octyl group to model the propagating chain and to highlight the mode by which the growing chain interacts with the binuclear catalyst. Although the polymer molecular weight, on passing from

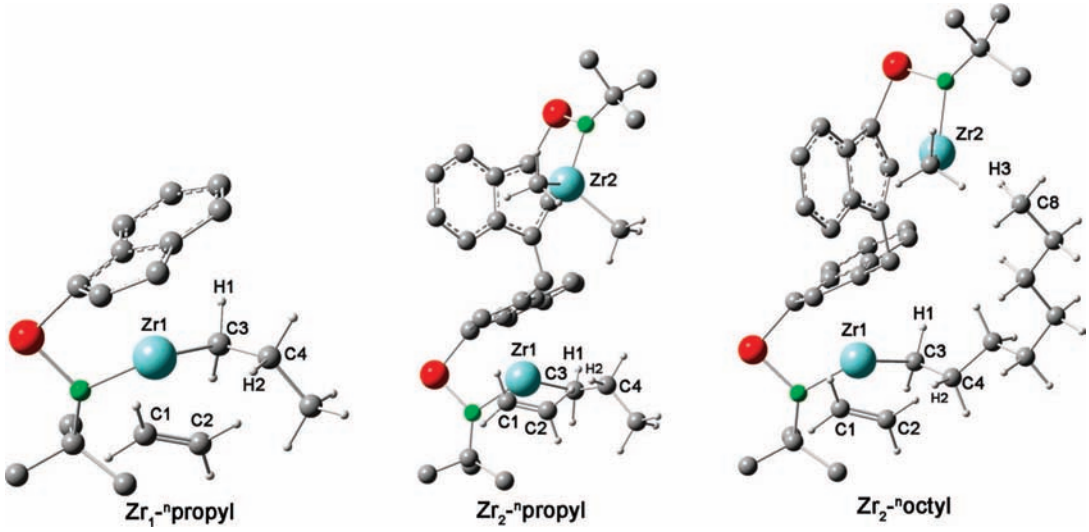

Figure 4. Olefin π-complex structures in the monometallic CGCZr- catalyst case with an ^{n}propyl growing chain ($\mathbf{Zr_1}$-^{n}propyl) and in the -CH_2- bridged bimetallic case with an ^{n}propyl growing chain ($\mathbf{Zr_2}$-^{n}propyl) and with an ^{n}octyl growing chain ($\mathbf{Zr_2}$-^{n}octyl).

Scheme 4. Energetic Profiles (kcal/mol) Describing Propagation and Termination Pathways for Ethylene Homopolymerization at the Indicated Mononuclear and Binuclear Catalyst Centers.

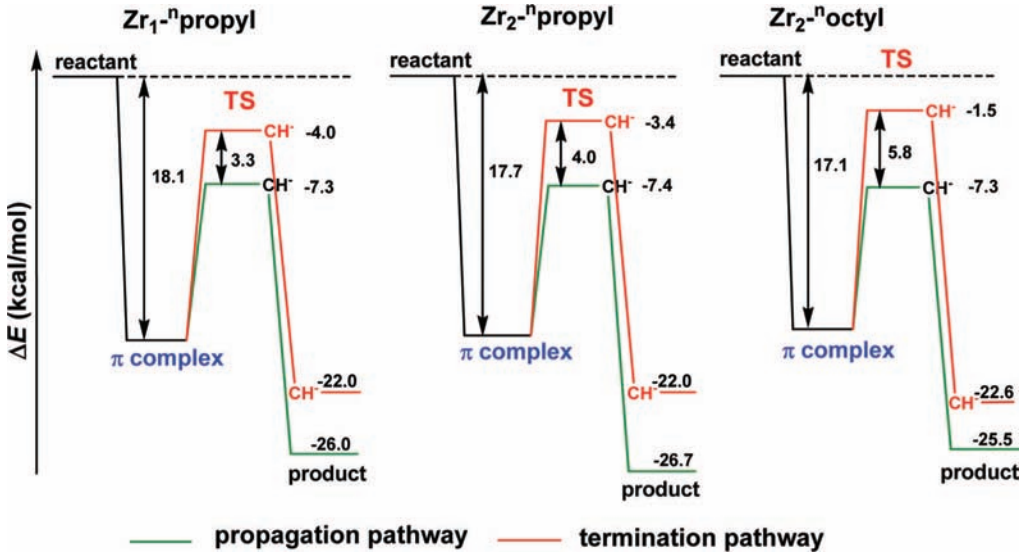

mononuclear $\mathbf{Zr_1}$ to binuclear $\mathbf{Zr_2}$ systems, is quantitatively modulated by the nature of the cocatalyst (MAO exhibits a stronger effect than the bis(borane) cocatalysts), the qualitative experimental trends are the same and argue that the increased polymer molecular weight is closely associated with the proximity effects of the two metal catalyst centers. Counteranion effects are, hence, not considered in this first level of analysis.

Both the initial enchainment and chain transfer processes are found to involve conventional π-complex formation between one metal site and the ethylene monomer (Scheme 3) at both the $\mathbf{Zr_1}$ and $\mathbf{Zr_2}$ catalysts. In the resulting π-complexes, a classic β-agostic interaction between the growing Zr-polymeryl chain and the active metal site is located as the low-energy conformation (Figure 4). Note that the computed values of the Zr1−C3−C4 angle (∼91.4°) and of the C4−H2 bond length (∼1.14 Å) suggest a distortion of the polymeryl chain well-tuned with the formation of a β-agostic interaction (Table 2). However, in the binuclear species, the longer ^{n}octyl chain (Zr_2-^{n}octyl) has an additional agostic interaction between the H3−C8 bond and the Zr2 site (Figure 4).

The nature of the present agostic interactions was thoroughly described in the previous section, and no further analysis need be carried out here. The data in Table 2 indicate that in the $\mathbf{Zr_1}$-^{n}propyl and $\mathbf{Zr_2}$-^{n}propyl cases, the geometrical environments around the Zr1 catalytic site are very similar. In particular, comparable computed Zr−C distances involving the C=C group π-coordinated to the Zr1 site (note the Zr1−C2 and Zr1−C3 bond lengths in Table 2) are found. In the binuclear catalyst, the longer growing ^{n}octyl chain ($\mathbf{Zr_2}$-^{n}octyl) slightly displaces the ethylene molecule from the Zr1 catalytic site. Thus, longer Zr1−C2 and C2−C3 distances are found (Table 2). These results find a counterpart in the steric hindrance arising from the C8−H3 agostic interaction with the Zr2 metal site that visibly constrains the ^{n}octyl fragment. Furthermore, the longer distances to the coordinated C=C bond result in a shorter Zr1−H2 distance (Table 2) in order to saturate the electrophilic Zr center. In energetic terms, the increasing steric hindrance on passing from $\mathbf{Zr_1}$-^{n}propyl, to $\mathbf{Zr_2}$-^{n}propyl and to $\mathbf{Zr_2}$-^{n}octyl incurs slight destabilization of the corresponding π-complexes (Scheme 4).

Insertion Pathways. The insertion transition states in all cases involve approach of the ethylene monomer to form a coplanar four-center (Zr1−C1−C2−C3) bonding framework (Figure 5). The elongation of the C3−H1 bonds (to 1.13 Å) and the distortion of the Zr1−C3−H1 angle (to ∼69°) from tetrahedral

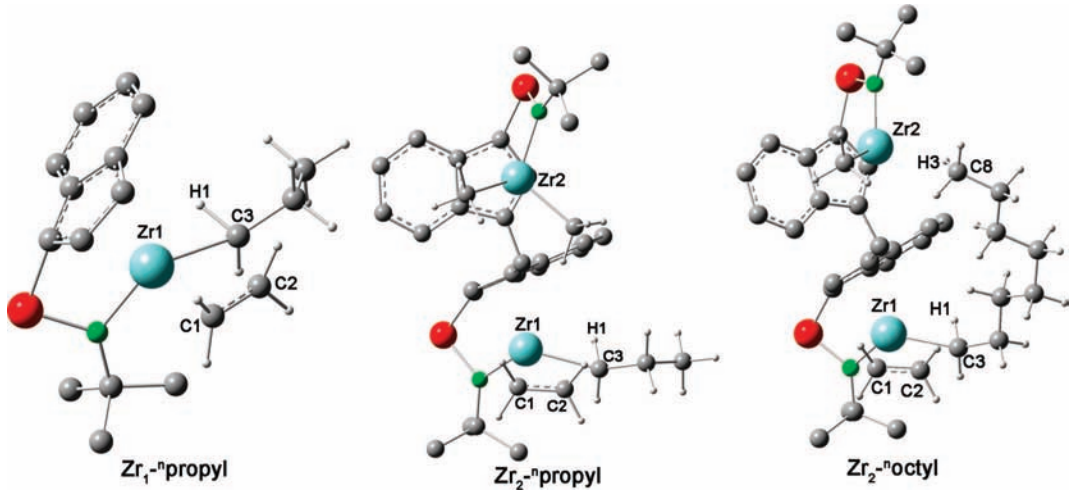

Figure 5. Transition-state structures computed for ethylene insertion pathways at the monometallic catalyst with an ^{n}propyl growing chain ($\mathbf{Zr_1}$-^{n}propyl) and in the -CH_2- bridged bimetallic catalyst having an ^{n}propyl growing chain ($\mathbf{Zr_2}$-^{n}propyl), and with an ^{n}octyl growing chain ($\mathbf{Zr_2}$-^{n}octyl).

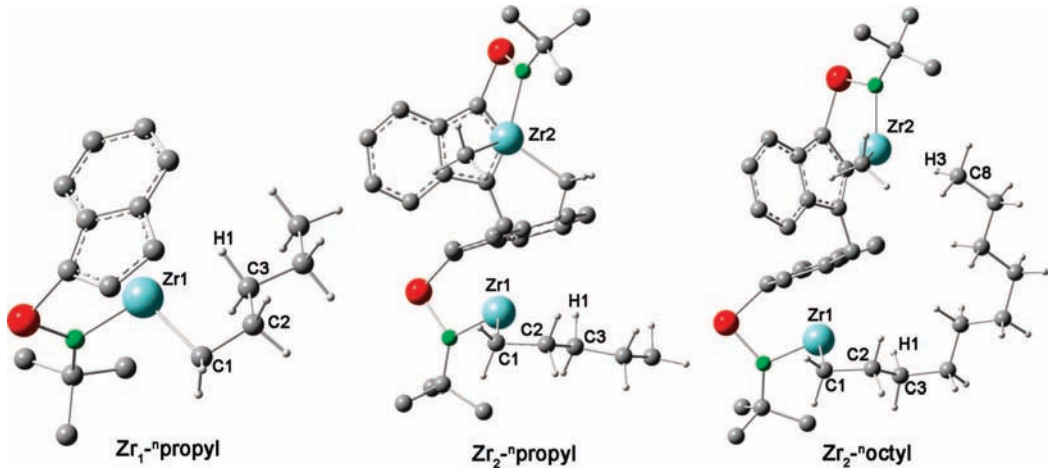

Figure 6. Kinetic product structures obtained from the ethylene insertion pathway in the monometallic CGC catalyst with an ^{n}propyl growing chain (**Zr$_1$**-^{n}propyl) and in the -CH_2- bridged bimetallic CGC catalyst with an ^{n}propyl growing chain (**Zr$_2$**-^{n}propyl), and with an ^{n}octyl propagating chain (**Zr$_2$**-^{n}octyl).

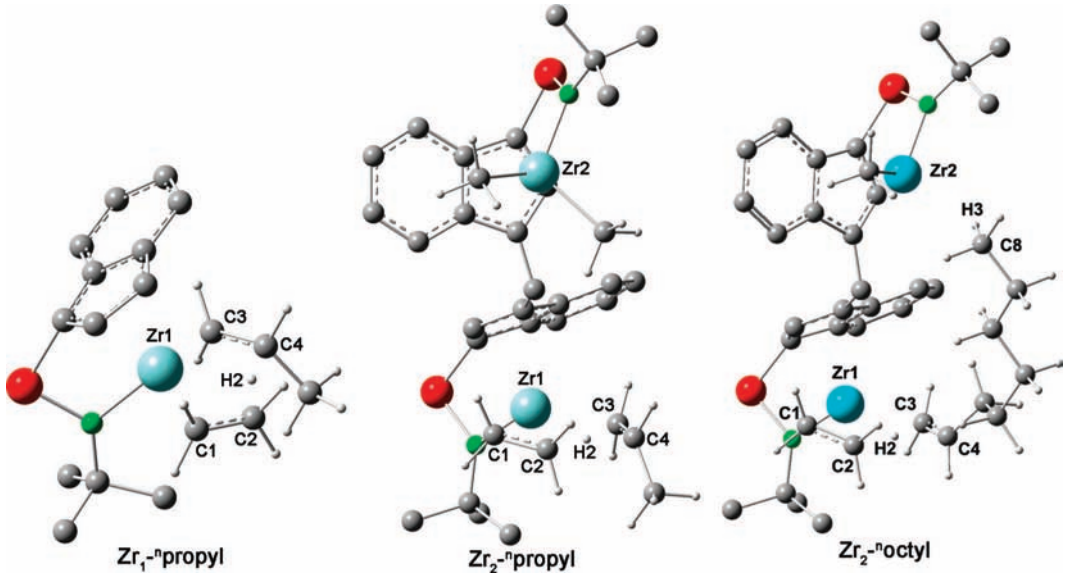

Figure 7. Transition-state structures for the chain transfer pathway in the monometallic CGC catalyst with a growing ^{n}propyl chain (**Zr$_1$**-^{n}propyl) and in the -CH_2- bridged bimetallic CGC catalysts with growing ^{n}propyl (**Zr$_2$**-^{n}propyl) and ^{n}octyl chains (**Zr$_2$**-^{n}octyl).

(109.5°) are, in all cases, indicative of α-agostic interactions that stabilize/preorganize the overall insertion process. The β-agostic interaction involving the C4−H2 bond and the Zr1 active center observed in the π-complexes of Figure 4 is lost in all cases.

The data in Table 2 reveal that there are no important geometrical differences between the mononuclear and binuclear ethylene insertion scenarios since the proximity of the second catalytic center and the nonbonded repulsion of the ^{n}octyl fragment constrained by the agostic interaction with the Zr2 site (Figure 5) do not significantly influence the Zr1 site geometrical environment in the transition states. In particular, the C2−C3 distance decreases on passing from **Zr$_1$**-^{n}propyl to **Zr$_2$**-^{n}propyl and to **Zr$_2$**-^{n}octyl, while the Zr1−C3 and C1−C2 distances increase (Table 2). These metrical trends do not significantly influence the stabilization of the transition-state structures. In fact, Scheme 4 shows similar energetic values (−7.3 to −7.4 kcal/mol) of the transition-state structures on passing from the **Zr$_1$**-^{n}propyl to the **Zr$_2$**-^{n}propyl and to **Zr$_2$**-^{n}octyl systems. The insertion pathways in all cases lead to Zr1−C1 and C2−C3 bond formation, simultaneous with scission of the Zr1−C3 bond (Figure 6). In this case, a γ-agostic interaction is operative. This result is tuned well with the observed elongation (to 1.12 Å) of the C3−H1 bond and distortion of the Zr1−C1−C2 angles (from 95.7° to 102.3°). The data in Table 2 reveal that no particular differences are evident on passing from the mononuclear **Zr$_1$**-^{n}propyl to the binuclear **Zr$_2$**-^{n}propyl catalytic system. In the case of Zr_2-^{n}octyl, the propagating chain configuration is slightly distorted with respect to **Zr$_1$**-^{n}propyl and **Zr$_2$**-^{n}propyl due to the C8−H3 agostic interaction with Zr2. This is consistent with the expanded values of the Zr1−C2 and Zr1−C3 distances and the Zr1−C1−C2 angle (Table 2) observed in the **Zr$_2$**-^{n}octyl case.

***β*-Hydrogen Chain Transfer Pathway.** In the chain transfer transition states, a concerted bond-forming/-breaking process,

(23) (a) Lanza, G.; Fragalà, I. L.; Marks, T. J. *Organometallics* **2002**, *21*, 5594–5612. (b) Lanza, G.; Fragalà, I. L.; Marks, T. J. *Organometallics* **2001**, *20*, 4006–4017.

(24) (a) Cossee, P. *J. Catal.* **1964**, *3*, 80–88. (b) Arlman, E. J.; Cossee, P. *J. Catal.* **1964**, *3*, 99–104.

Table 3. Computed Geometrical Parameters in the π-Complexes, Chain Transfer Transition States, and Products for the Chain Transfer of Ethylene at the Indicated Mononuclear and Binuclear CGCZr Catalysts

	Chain Transfer Path		
	Zr_1-^{n}propyl	Zr_2-^{n}propyl	Zr_2-^{n}octyl
		π-Complex	
Zr1−C1	2.836	2.839	2.845
Zr1−C2	2.863	2.857	2.897
Zr1−C3	2.236	2.236	2.245
Zr1−C4	2.736	2.740	2.736
Zr1−H2	2.318	2.324	2.303
C4−H2	1.141	1.140	1.145
C2−H2	2.534	2.548	2.452
C1−C2	1.348	1.348	1.348
C3−C4	1.520	1.521	1.520
Zr1−C3−C4	91.5	91.6	91.1
		Transition State	
Zr1−C1	2.441	2.440	2.443
Zr1−C2	2.670	2.673	2.711
Zr1−C3	2.413	2.413	2.536
Zr1−C4	2.712	2.713	2.896
Zr1−H2	2.045	2.052	1.986
C4−H2	1.516	1.511	2.002
C2−H2	1.538	1.538	1.680
C1−C2	1.404	1.404	1.402
C3−C4	1.413	1.414	1.376
		Kinetic Product	
Zr1−C1	2.227	2.231	2.215
Zr1−C2	2.774	2.764	3.425
Zr1−C3	2.718	2.725	2.661
Zr1−C4	3.087	3.107	3.258
Zr1−H2	2.431	2.412	3.722
C4−H2	2.630	2.602	5.810
C2−H2	1.127	1.128	1.096
C1−C2	1.530	1.529	1.529
C3−C4	1.354	1.354	1.356
Zr1−C1−C2	93.3	92.8	131.5

paralleling the hydrogen transfer, is active between Zr1 and carbon atoms C1/C3, respectively (Figure 7). At this point, the C1−C2 and C3−C4 bond lengths exhibit intermediate values between single and double bonds. Furthermore, the transition state is stabilized by a Zr1−H2 agostic interaction. In the **Zr_1**-^{n}propyl and **Zr_2**-^{n}propyl catalysts, the computed C4−H2 and C2−H2 distances lie very close to 1.51 Å (Table 3), thus indicating a symmetrical hydrogen transfer process.

In the **Zr_2**-^{n}octyl case, the C4−H2 and C2−H2 distances have values of 2.00 and 1.68 Å, respectively (Table 3). Here the increased steric repulsions associated with the particular conformation of the propagating ^{n}octyl chain (constrained by the agostic interaction with the second metal center), destabilizes the structure and precludes significant relaxational rearrangement. These steric effects will be more evident in the product structures. In terms of energetics, the **Zr_1**-^{n}propyl and **Zr_2**-^{n}propyl transition-state structures exhibit similar values, with slight destabilization evident in the **Zr_2**-^{n}propyl case (due to nonbonded repulsions), while the **Zr_2**-^{n}octyl case exhibits more consistent destabilization (Scheme 4), in agreement with the geometrical considerations discussed above. The chain transfer process leads to the formation of a linear alkene (in this case, propene for the **Zr_1**- and **Zr_2**-^{n}propyl catalysts and ^{n}octene for the **Zr_2**-^{n}octyl case) coordinated at the Zr1 center and an ethyl fragment bonded to the Zr1 metal center (Figure 8).

In the **Zr_1**- and **Zr_2**-^{n}propyl cases, β-agostic interactions are active between the ethyl fragment and the metal center (Figure 8). The computed Zr1−C1−C2 angle distortion and the C2−H2 bond elongation (Table 3) agree well with this observation. In the case of **Zr_2**-^{n}octyl, rotation of the ethyl fragment around the Zr1−C1 bond is observed, followed by the scission of the C2−H2 β-agostic interaction (Figure 8, Table 3). In this case, the ethyl fragment rearrangement is due to the steric hindrance around the Zr1 catalytic site, associated with the ^{n}octyl fragment and amplified by this constrained configuration, reflecting both olefin coordination to the Zr1 site and the C8−H3 agostic interaction at the Zr2 site.

This rearrangement of the ethyl fragment in the product affords an energetically more relaxed configuration versus the **Zr_1**-^{n}propyl and **Zr_2**-^{n}propyl structures (Scheme 4). Note that the conformation of the chain transfer product in the **Zr_2**-^{n}octyl case is well positioned for the reinsertion process, since the insertion pathway involves breaking the β-agostic interaction (vide supra).

Overall, the above energetic analysis reveals that the insertion activation barrier is only moderately influenced by the **Zr_2** metal−metal proximity arising from a second catalytic CGCZr-site as well as by nonbonded repulsions involving the ^{n}octyl fragment (Scheme 4). In marked contrast, the cooperative effects of the second proximate metal center and of the growing polymer chain (modeled here by the ^{n}octyl fragment) significantly influence the kinetics of the chain transfer process and progressively increase the activation barrier with increasing catalyst nuclearity and poly/oligoethylene chain length (Scheme 4). It is therefore found that, in comparison to the monometallic analogues, the bimetallic CGCZr catalyst systems favor olefin insertion over chain transfer and, hence, propagation over chain termination. This behavior is closely linked with the specific configuration of the growing polymer chain (^{n}octyl fragment) and the resulting C8−H3 agostic interaction with the second Zr center, and is in accord with the generally increased polymer molecular weight observed experimentally on proceeding from mononuclear to binuclear catalysts.[6a−c,9] Furthermore, the geometrical configuration of the chain transfer process product is well positioned for reinsertion, which would yield the experimentally observed ethyl chain branching.[9] The diminished **Zr_2** chain transfer rate obviously does not favor ethyl branch formation (Scheme 1). In fact, there is experimental evidence that the polyethylene ethyl branch densities scale roughly inversely with the product molecular weights from the various binuclear catalytic systems.[9b] Thus, higher molecular weights correlate with lower ethyl branch densities due to the aforementioned role of the chain transfer step in the ethyl branch formation. In the case of **C2−Zr_2** and **Zr_2** with MAO as cocatalyst, the reduced chain transfer activity (the polyethylene molecular weight is enhanced ~600× with respect to the mononuclear catalyst product) probably precludes the ethyl branch formation.[9b] In the other cases, where the reduced chain transfer is less evident, the enhanced probability of the reinsertion step (Scheme 1) analyzed in the previous section, likely represents the principal source of ethyl branch formation.

Concluding Remarks

Proximity effects in (μ-CH_2-3,3′){(η^5-indenyl)[1-H_2Si(^{t}BuN)]-($ZrMe_2$)}$_2$ (**Zr_2**)-derived catalysts which are operative during ethylene polymerization processes have been scrutinized using density functional theory. In particular, attention was focused on ion-pair formation/interaction between both binuclear **Zr_2** precatalyst diastereoisomers (*R,R* and *R,S*) and the binuclear bis(borane) cocatalyst 1,4-$(C_6F_5)_2BC_6F_4B(C_6F_5)_2$ (**BN_2**). It is found that complete methyl abstraction produces four possible

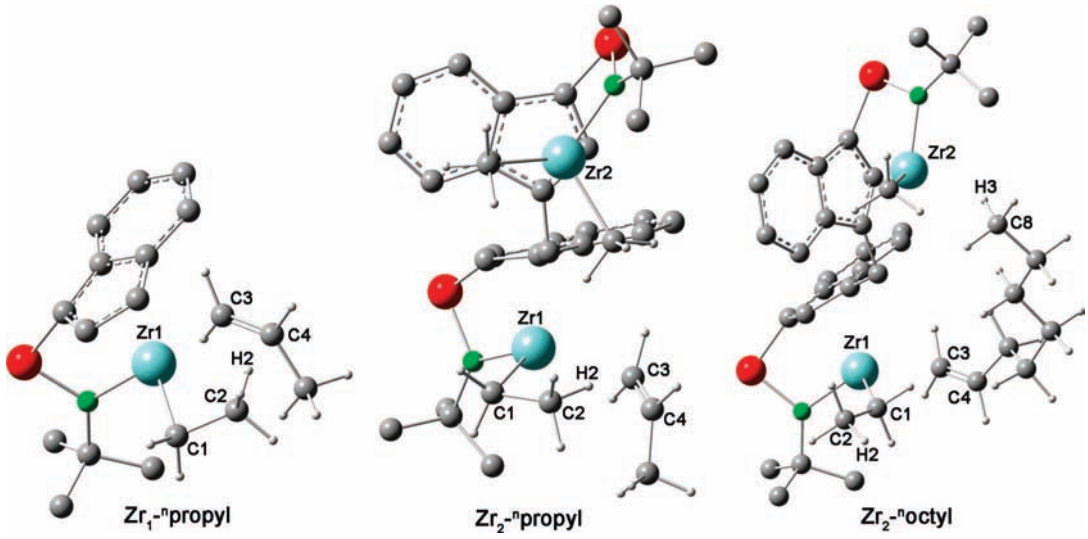

Figure 8. Kinetic product structures obtained from the chain transfer pathway in the monometallic CGC catalyst with a growing ^{n}propyl chain (**Zr$_1$**-^{n}propyl), in the -CH_2- bridged bimetallic CGC catalyst with an ^{n}propyl growing chain (**Zr$_2$**-^{n}propyl), and with an ^{n}octyl growing chain (**Zr$_2$**-^{n}octyl).

structures, dictated by geometrical constraints. Comparison of energetic data for the ion-pair interactions in the mononuclear and binuclear catalyst cases suggests that the ion-pair stabilization energy depends largely on geometrical matching between the interacting ion-paired fragments and explains the experimentally observed depressed polymerization activity of the binuclear CGC systems relative to the mononuclear CGC analogues. Moreover, the present theoretical results accurately describe and provide important geometrical details concerning agostic interactions between the growing chain interacting at one **Zr$_2$** metal site while propagating from the second proximate metal site. These observations are in accord with experiment which indicates enhanced ethyl branch formation in the binuclear catalyst-mediated polymerization processes. Finally, the energetics of the insertion step, associated with the polymerization propagation pathway, are compared with the chain transfer step, associated with the polymerization termination pathway, in the mononuclear versus binuclear CGC catalysts. It is found that the proximity of the second **Zr$_2$** metal center only slightly influences the insertion process kinetics, but significantly depresses the rate of chain transfer and, hence, that of the chain growth termination process. This behavior explains the increased polymer molecular weights observed, in good agreement with experiment.

Acknowledgment. This research was supported by the Ministero dell'Istruzione, dell'Università e della Ricerca (MIUR Rome), the Consiglio Nazionale delle Ricerche (CNR Rome), and by the U.S. Department of Energy (Grant 86ER13511).

Supporting Information Available: Geometric and energetic comparison between binuclear and mononuclear precatalysts and between the related naked cations; complete ref 21; a complete list of Cartesian coordinates of all structures presently analyzed. This material is available free of charge via the Internet at http://pubs.acs.org.

JA8077208